ELSEVIER

Physics of the Earth and Planetary Interiors 89 (1995) 109–125

PHYSICS OF THE EARTH AND PLANETARY INTERIORS

# The 1977 Three Kings Ridge earthquake ( $M_s = 6.7$): broad-band aspect of the source rupture

Fumiko Tajima [a,*], Emile A. Okal [b]

[a] *Institute for Geophysics, University of Texas at Austin, Austin, TX 78759-8397, USA*
[b] *Department of Geological Sciences, Northwestern University, Evanston, IL 60208, USA*

Received 3 January 1994; revision accepted 25 August 1994

**Abstract**

The 1977 Three Kings Ridge earthquake ($M_s = 6.7$) is an isolated event which took place in the South Fiji Basin. The centroid moment tensor (CMT) solution by the Harvard group shows a left-lateral strike-slip motion with a dip angle of 55° while the P-wave first motions require a nearly vertical fault plane. The centroid depth 17.4 km is deeper than the bottom of ordinary oceanic crust.

Using long-period P and SH waveforms from the Worldwide Standardized Seismograph Network, we model the entire source rupture process with three subevents which span a 42 s duration. The best-fit double-couple focal mechanism obtained from the tensorial sum of the subevents is primarily a strike-slip with a nearly vertical fault plane subparallel to the Cook Fracture zone. The total moment release is $(2.2–2.3) \times 10^{26}$ dyn cm, which is about 40% lower than the CMT estimate. The subevents' depth distribution is similar to the centroid depth (17 km), which is deeper than a typical oceanic Moho. Precise modeling of the waveforms is also incompatible with a standard oceanic crustal structure, lending support to previous interpretations of the Three Kings Ridge as a fossil island arc.

The discrepancy between our body waveform moment tensor solution and the Harvard CMT solution is dominated by the tensor components $M_{r\theta}$ and $M_{r\phi}$. In the case of a shallow source, these components are notoriously unresolvable because of their vanishing excitation of seismic waves in the low-frequency range ($T \geqslant 45$ s). However, the low-pass filtered body waves can be better modeled with a dip angle similar to that of the CMT solution. This observation suggests that the source process may include some level of evolution of the rupture mechanism with time. We interpret the earthquake as expressing a moderate level of internal deformation of the Australian plate, in the context of significantly different spreading rates in the Lau and Havre Basins.

## 1. Introduction

The South Fiji Basin is a large oceanic basin which opened as the back-arc basin of the Tonga–Kermadec subduction system during the Oligocene. The bathymetry, shown in Fig. 1(a), suggests that the basin is separated into two distinct parts by an eastward extension of the Cook Fracture Zone. The southern section of the basin is bounded by the Three Kings Ridge and has only about half the width of the northern section (Malahoff et al., 1982). Packham and Terrill (1975) named the two sub-basins the Kupe

* Corresponding author.


*SSDI* 0031-9201(94)02998-9

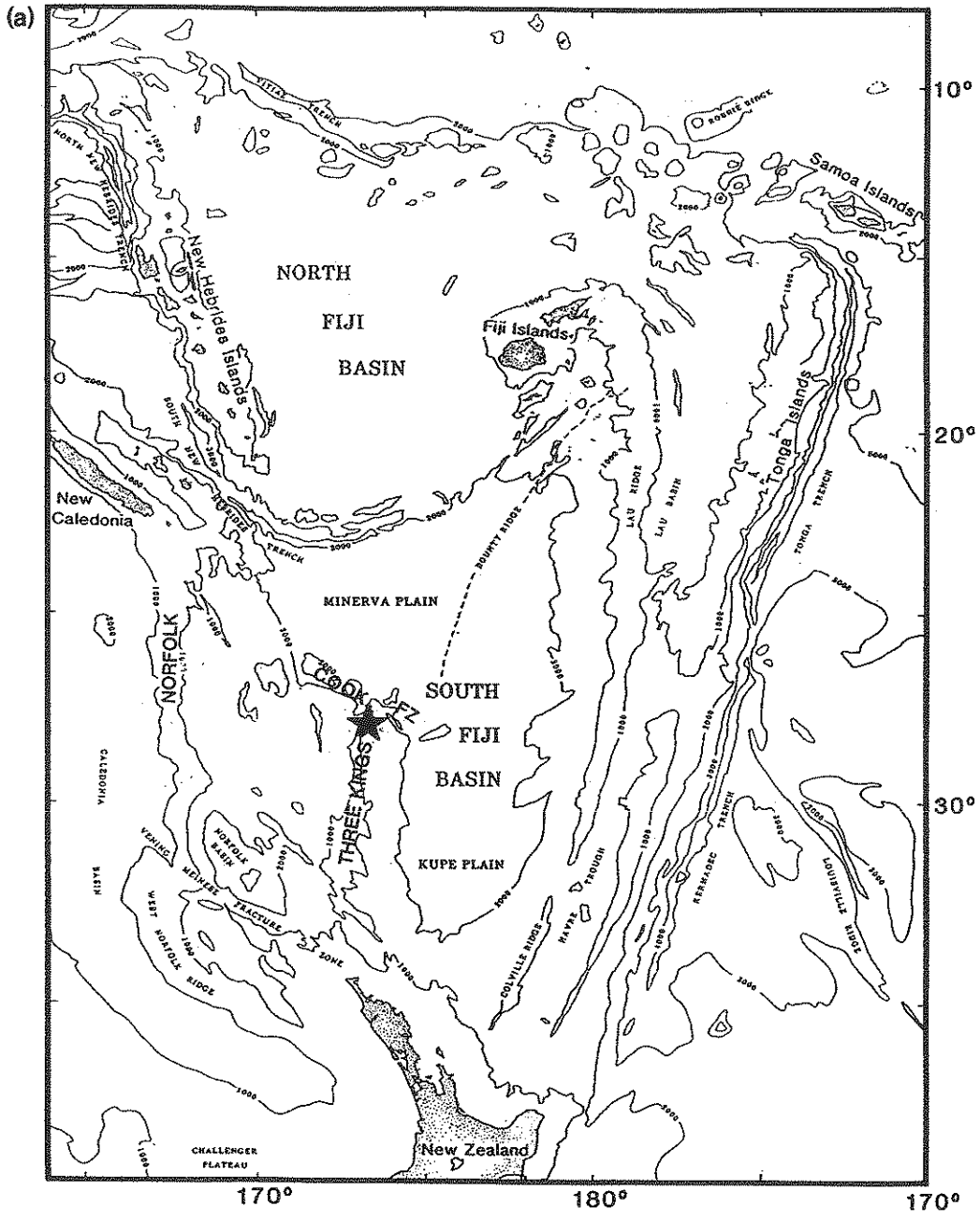


Fig. 1. (a) Map of the principal bathymetric and tectonic features of the inter-arc basins north of New Zealand based on Mammerickx et al. (1974) (slightly modified from Malahoff et al. (1982). (b) Seismicity of South Fiji Basin and adjoining area superimposed on SYNBAPS bathymetry. The plate boundary seismicity represents all events in the NEIC catalog for the period 1963–1992. Inside the dashed box, the intraplate seismicity is taken from Valenzuela and Wysession (1993), and shown as triangles. The large triangle is the 17 October 1977 Three Kings event whose focal mechanism is determined in the present study (large beachball); the nearby black triangles represent its aftershocks. The other four focal mechanisms are those available from the CMT catalog (small beachballs). The inverted triangles (with date) are the historical earthquakes with magnitudes larger than six.

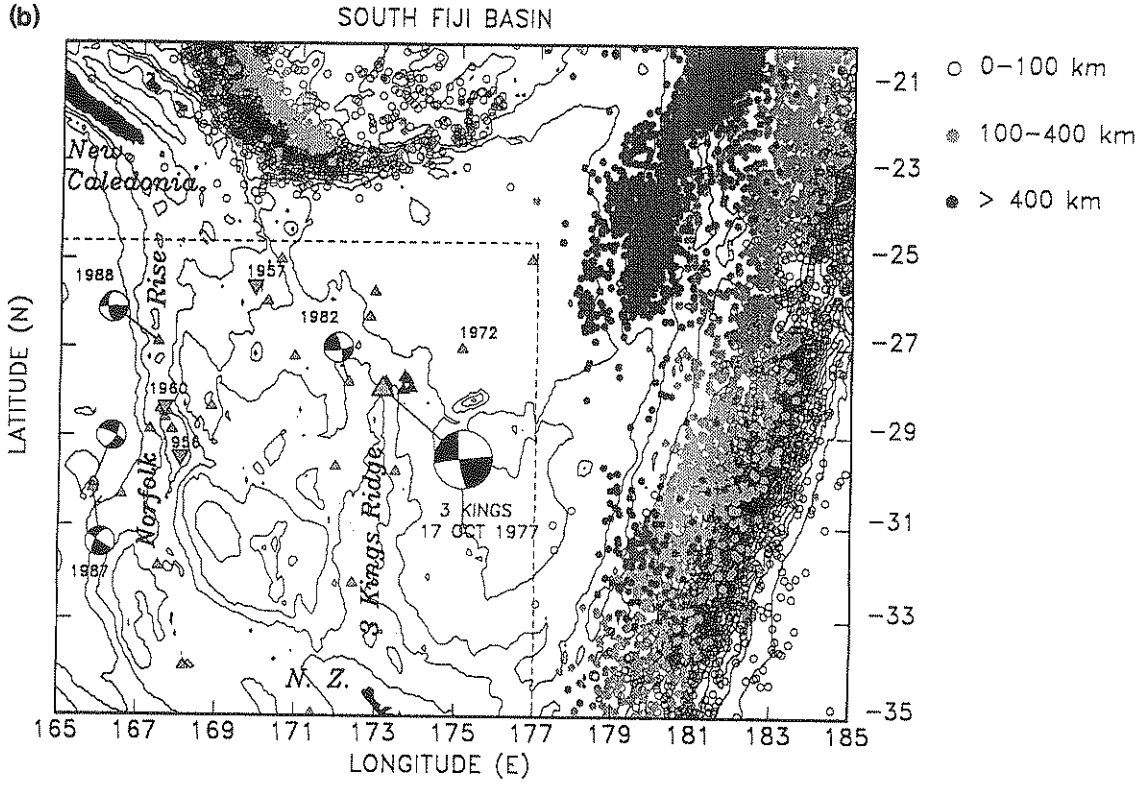


Fig. 1 (continued).

Abyssal Plain to the south and the Minerva Abyssal Plain to the north, based on a detailed bathymetry map. Early interpretations of the Three Kings Ridge favored a fossil spreading center (Van der Linden, 1969), but seismic reflection and magnetic data advocate an island arc structure (Karig, 1972; Coleman and Packham, 1976; Launay et al., 1982). Furthermore, Kroenke and Dupont (1982) have interpreted the Three Kings Ridge as a west-facing island arc under which a significant amount of Norfolk Basin lithosphere may have been subducted.

In this basin a major earthquake occurred at the northern end of the Three Kings Ridge on 17 October, 1977. Its assigned magnitudes were $m_b = 6.3$; $M_s = 6.7$; $M_{PAS} = 6.9$. This event, shown as the large triangle in Fig. 1(b), was followed by eight aftershocks (four of which had $m_b \geq 4.9$) over a period of 5 months. Otherwise, the intraplate seismicity of the South Fiji Basin is very low: in Fig. 1(b), subduction zone events, plotted as dots, are taken without relocation from the National Earthquake Information Center (NEIC) catalog for the period 1963–1992. Inside the box outlined by dashes, the intraplate seismicity, plotted as triangles, is taken from the recent relocations of Valenzuela and Wysession (1993), and covers the years 1918–1992, even though the earliest confirmed earthquake in this area occurred in 1956. As discussed in detail below, the background seismicity is at a considerably lower level than the 1977 earthquake sequence, with all events from 1963 to present featuring $m_b \leq 5.6$. It should be noted also that most of the South Fiji Basin intraplate seismicity is concentrated on the Norfolk Rise, which extends from New Zealand to New Caledonia, and on the Three Kings Ridge–Cook Fracture Zone system. It is clear that the combination of the size of the 1977 Three Kings earthquake and its intriguing location gives it a unique character and warrant a more detailed study.

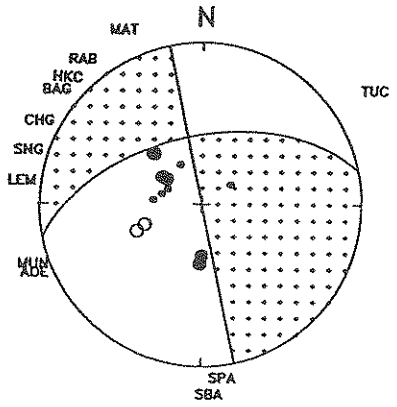


Fig. 2. Lower hemisphere equal-area projection of P-wave first-motion arrivals (●, compression; ○, dilatation) read from WWSSN records, superimposed on the CMT solution as determined by the Harvard group. The polarities with small amplitudes are shown by small circles. These first motions indicate a much steeper dip angle than, and a different rake from the CMT solution.

The best-fitting double-couple focal mechanism of the main event determined by centroid moment tensor (CMT) inversion, and listed in the Harvard catalog (Dziewonski et al., 1987) is an oblique strike-slip mechanism. The source parameters are strike $\phi = 258°$, dip $\delta = 55°$, rake $\lambda = 0°$; the centroid depth 17.4 km; and the released moment $M_0 = 3.7 \times 10^{26}$ dyn cm (see Fig. 2). The east–west direction of slip and the strike of the inclined fault plane are similar to the orientation of the Cook Fracture Zone. However, this solution is controversial both from seismological and tectonic perspectives:

(1) the fault plane, presumed to be along the Cook Fracture Zone, is dipping at a relatively shallow angle (55°);

(2) the CMT source depth is below the bottom of ordinary oceanic crust;

(3) this event location is isolated from the other major events in the South Fiji Basin;

(4) more importantly, the P-wave polarities read from long-period records at several World Wide Standardized Seismographic Network (WWSSN) stations are inconsistent with the above best-fitting double-couple CMT mechanism (see Fig. 2).

The Harvard CMT solution was determined using long-period body and mantle waves ($T \geqslant 45$ s). Accordingly, its oblique strike-slip focal mechanism represents the long-period behavior of the source rupture whereas the polarities read from WWSSN long-period records correspond to the radiation pattern of the rupture at the relatively short period characteristic of unfiltered WWSSN body-wave records (typically 20 s or shorter). The inconsistency between the P-wave polarities and the CMT solution suggests that the source mechanism may have changed during the process.

Although intraplate oceanic seismicity is known to take place below the Mohorovičić (Moho) discontinuity (Bergman and Solomon, 1980; Wiens and Stein, 1983), it is important to explore the possibility of an abnormally thick crust in this region. This would be suggested by the argument that the Three Kings Ridge has an island arc structure (Kroenke and Dupont, 1982; Kroenke and Eade, 1982). Finally, if the earthquake involves a change of mechanism during the rupture, we may have to invoke a bending rupture zone. The purpose of this paper is to obtain a revised moment tensor solution of this intriguing intraplate earthquake by determining its detailed source time process. We then discuss tectonic implications based on our seismological study.

## 2. Seismological perspectives

As we mentioned above, the first-motion arrivals read from WWSSN long-period seismograms are inconsistent with the best-fitting double-couple focal mechanism of the Harvard CMT solution (Fig. 2). In Fig. 3, we show digitized P waveforms, rescaled to a common magnification of 1500. The original magnification is 750 at Stations SPA, ADE, MUN, LEM, HKC and RAB, 1500 at TUC and SBA, and 3000 at SNG, CHG, BAG and MAT. The theoretical P-wave arrival time calculated for the iasp91 Earth model (Kennett and Engdahl, 1991) is shown as a tick mark on each trace. These first-motion arrivals with a characteristic period of less than 20 s (e.g. recorded by the WWSSN long-period instruments) indicate a steeper dip angle than that of the CMT solution. The small amplitudes at TUC,

SNG, CHG, BAG, HKC and MAT are probably due to the locations near a nodal plane (shown with smaller circles on the focal sphere in Fig. 2). Stations SPA, SBA, ADE, MUN, LEM and RAB show clear polarities.

To explore the low-frequency features of the P-wave first motions, we applied a low-pass-band filter ($0.01 < f < 0.022$ Hz or $45 < T < 100$ s) to the dataset shown in Fig. 3. Here the starting points of the wavelets were set far before the theoretical arrival times to avoid affecting the waveshape through tapering. Fig. 4(a) shows the result. Compared with Fig. 3, the polarities at LEM, SBA, TUC, CHG, and SNG are reversed. This distribution of dilatational stations indicates a less steep dip angle than in Fig. 2 (see Fig. 4(b)). The amplitudes at TUC, SPA, SBA, CHG, SNG, BAG, and MAT are small, which may indicate their locations near the nodal planes. However, the dip angle of the fault plane inferred from the CMT solution remains far less steep than that estimated by these low-frequency P-wave polarities.

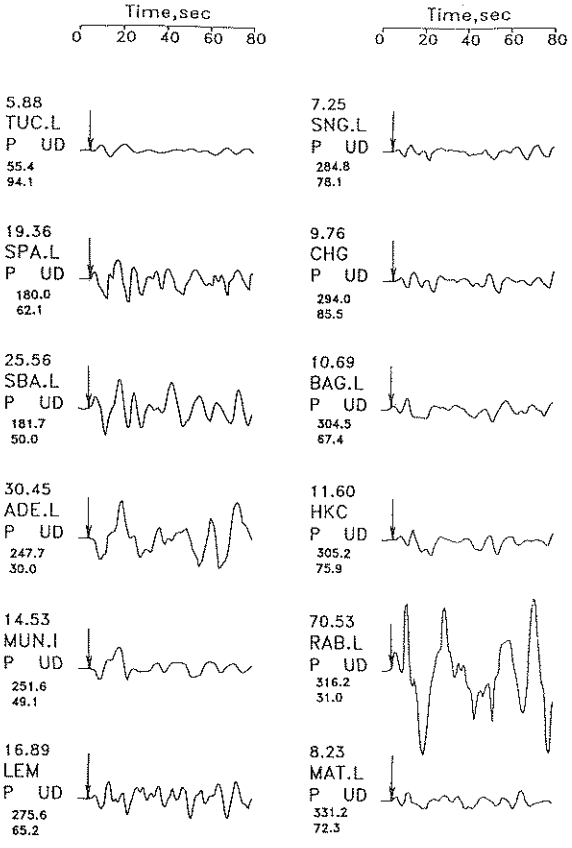


Fig. 3. P waveforms digitized and rescaled to a common magnification (1500). The peak-to-peak amplitude (cm), station identification, station azimuth (degrees), and distance (degrees clockwise from north) are shown on the left-hand side of each seismogram. The theoretical P-wave arrival time calculated with the iasp91 Earth model is tick marked for each trace.

The above observations suggest that the source process of the event may include some level of evolution of the focal mechanism with time, e.g. the mechanism of the rupture characterized by an almost vertical nodal plane at relatively high frequencies overlaps the mechanism with a less steep dip angle at low frequencies. The CMT depth of 17.4 km, which is deeper than an oceanic Moho, suggests that we should check whether an adequate crustal model is different from an ordinary oceanic model in this area. Fig. 5 illustrates the features implied from our preliminary check of this event schematically.

Although there exist various waveform inversion methods to investigate changes of mechanism in source time processes, instruments available in 1977 did not have the broad-band characteristics necessary for this purpose: the Global Digital Seismograph Network (GDSN) has instruments with very narrow band response, and its station coverage was poor at the time; the International Deployment of Accelerographs (IDA) instruments record only very-long-period vertical-component data and were, in 1977, sampling at 20 s. Finally, the dynamic range of the WWSSN long-period instruments is limited, making it difficult to invert seismic waves produced from a complex source which involves a broad frequency range. Under the circumstances, our analysis of the source rupture process is restricted to using the WWSSN long-period body waveforms.

## 3. Source-time process

We examine the source characteristics from teleseismic long-period P and SH waveforms recorded by WWSSN instruments whose peak

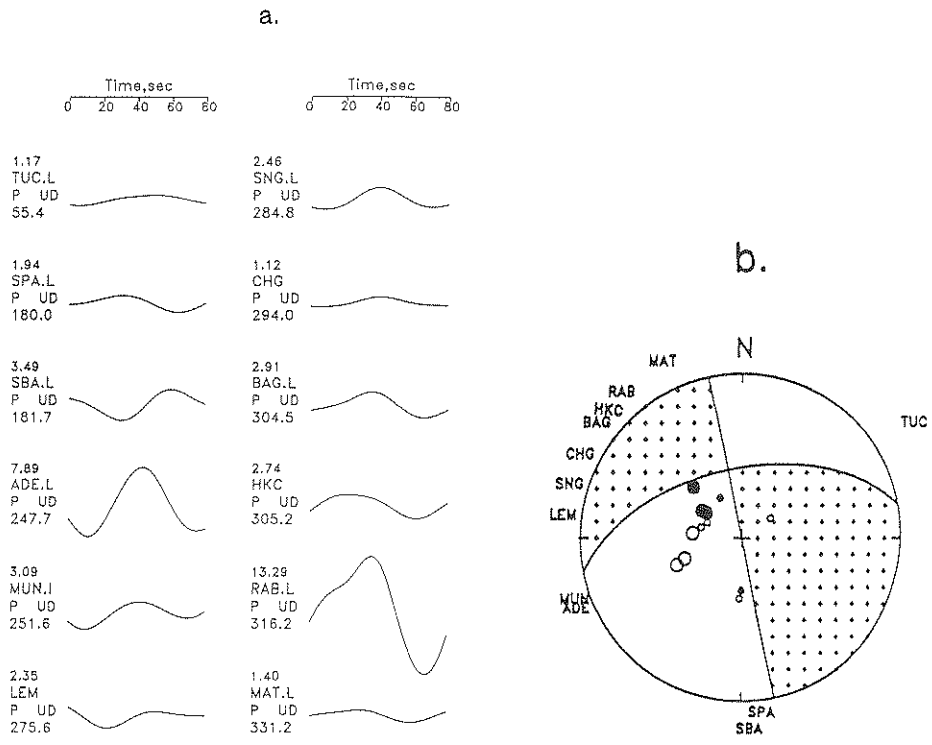


Fig. 4. (a) P waveforms after the low-pass-band filter was applied and the instrument response was removed. (Note that the polarities are reversed at Stations SBA and LEM.) (b) The polarities of the low-pass band filtered P waveform arrivals are shown on the focal sphere with the nodal planes of the CMT solution.

frequency responses are about 0.05 Hz. We adopt the iterative inversion method of Kikuchi and Kanamori (1991) to analyze the body waveforms. This method models the entire source process with a series of subevents allocated at grids and has the capability of determining the mechanism

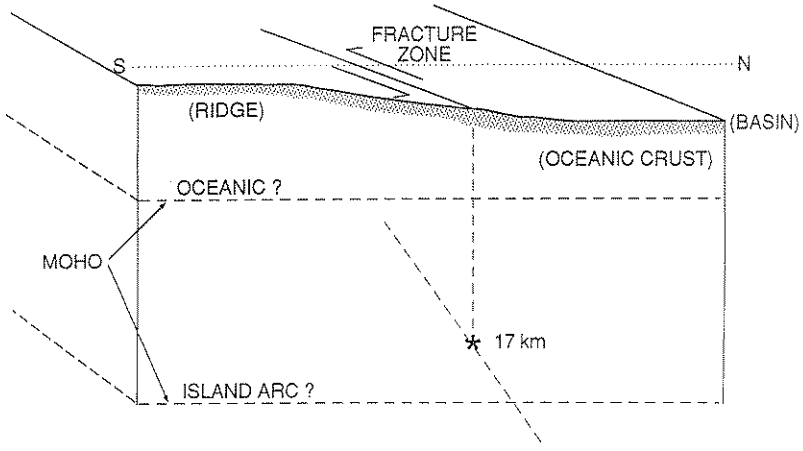


Fig. 5. Schematic illustration of the source rupture of the 1977 Three Kings Ridge earthquake inferred from the first-motion arrivals (e.g. almost a vertical fault plane with a strike parallel to the Cook Fracture Zone) and the CMT solution with an oblique strike-slip motion. An ordinary oceanic Moho and a possibly deeper Moho in this area are also indicated.

(e.g. moment tensor) of each subevent as well as its location and onset time. Here the moment tensor is determined as a combination of five deviatoric elementary moment tensor, and the coefficients of the elementary moment tensors as well as the other parameters are determined in a least-squares sense.

Initially, the grid points are set on a plane which is a potential fault area and has the same strike and dip angles as a preliminary mechanism solution such as obtained from the CMT solution, or from a first-motion mechanism solution. When the strike and dip angles of major subevents are substantially different from the grid geometry used initially, the inversion is performed again for the new grids taken on the plane with revised strike and dip angles. Before performing the inversion, we calculate a Green's function for each of the five deviatoric elementary moment tensors for all the grid points using an adequate near-source layered velocity structure, and the hypocentral location.

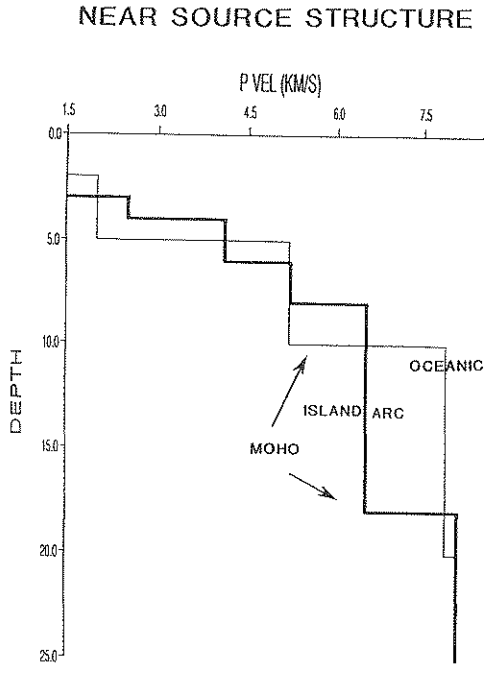


Fig. 6. Layered P-wave velocity structures for an ordinary oceanic crust model (thin line) and an island arc crustal model (bold line), respectively.

### 3.1. Test for an adequate near-source structural model

The near-source structural model used can have a substantial effect on the inversion results as well as the resolution of source depth, should crustal thickness be greater than several kilometers, in the case of an oceanic source. In the present case, our knowledge of crustal structure in the vicinity of the source is poor, and for this reason, we tested both an ordinary oceanic structure and a structure similar to an island arc with a crustal thickness of 18 km (see Fig. 6) by forward modeling the waveforms. Here we used a focal mechanism ($\phi = 258°$, $\delta = 82°$, $\lambda = 0°$) which has the same strike and rake as but a much steeper dip angle than the CMT solution, the centroid depth 17.4 km, and the moment $M_0 = 2.0 \times 10^{26}$ dyn cm. The source-time function is a simple triangle ($\tau_1$, $\tau_2 = 2$ s, 2 s). When computed for a typical oceanic structure, the agreement between the synthetics and data was poor. The fit was improved with the island arc structure. Fig. 7 shows the data (top) and a comparison of the corresponding synthetics calculated for the oceanic (bottom) and island-arc (middle) crustal models at several stations. Based on this experiment, our preferred model is the island arc structural model.

### 3.2. Inversion results

The grid depths were set at 7, 12, 17 and 22 km. We tested a variety of dip angles for the plane of grids between 55° and 87° which correspond to the dip angle of the CMT solution and that indicated from the first-motion arrivals in this study until stable solutions are obtained. Then we construct a series of subevents whose mechanisms as well as the locations and onset times are determined. This procedure allows us to unravel changes in focal mechanism during the rupture process.

For the island arc structure tested above the solutions are stable within the given range of dip angle for the grid plane, and the entire source process could be modeled with three subevents.

With a grid plane dip angle of 55°, as suggested by the CMT solution, the first and second subevents are located at a depth of 17 km, releasing the major part of the moment, $1.34 \times 10^{26}$ dyn cm and $1.3 \times 10^{26}$ dyn cm, respectively. Their mechanisms ($\phi = 263°$, $\delta = 87°$, $\lambda = 11°$, and $\phi = 272°$, $\delta = 85°$, $\lambda = 0°$, respectively) are very similar to each other; and the two foci were found 10 km and 4 s apart. The third subevent was found at a depth of 12 km, 40 km west of the first subevent, and 42 s from the onset of the rupture; its moment release is only $6.24 \times 10^{25}$ dyn cm, but its inclusion improves substantially the fit of the later part of P wavetrains, as well as SH waveforms. The source-time function and the subevent mechanisms are shown in Fig. 8(a). It should be noted that the third subevent mechanism ($\phi = 289°$, $\delta = 72°$, $\lambda = -173°$) is practically opposite to that of the first two, as can be observed from the reversed polarities of the later impulses in the seismogram, particularly notable at Stations LEM, RAB, MUN and BAG. The best double-couple solution obtained from the tensorial sum of the three subevent moments is a near-perfect strike-

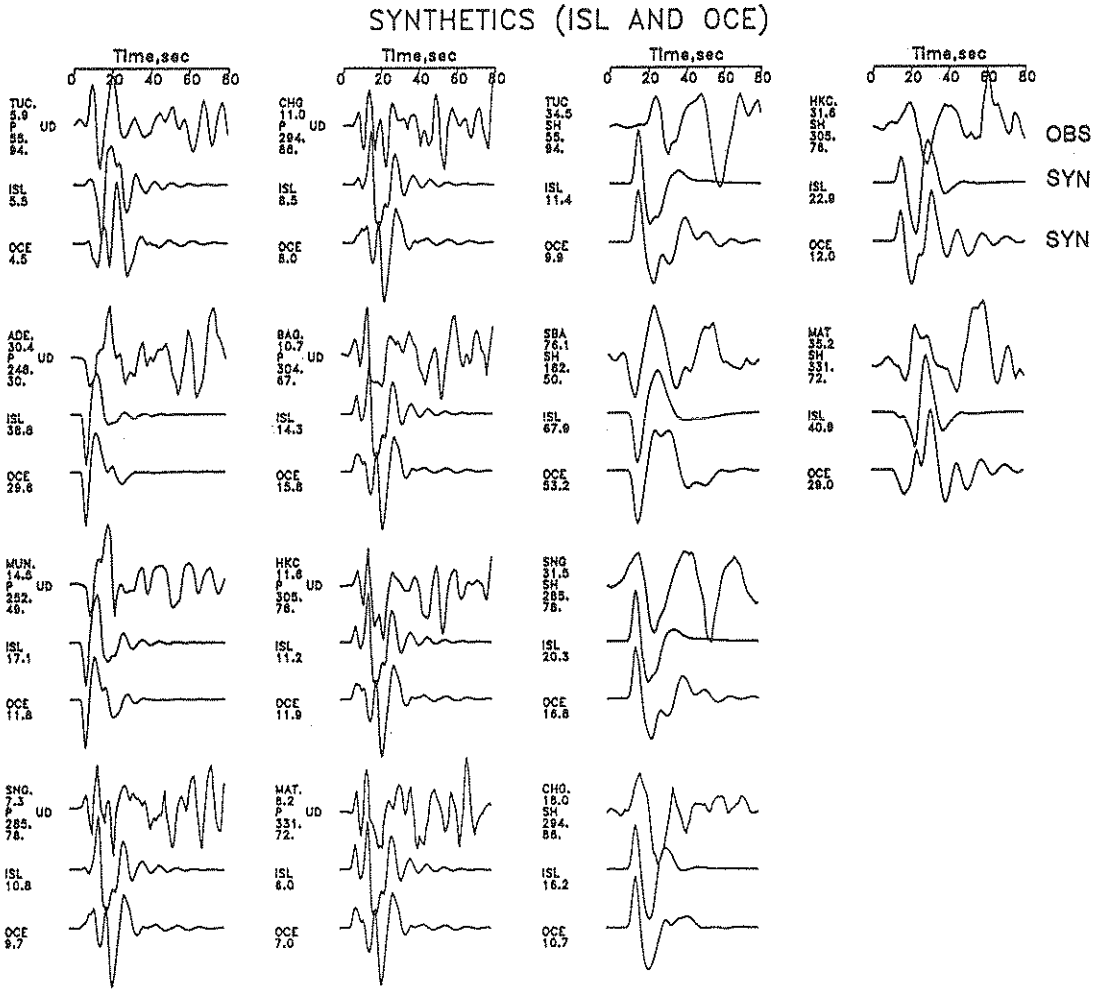


Fig. 7. Synthetic waveforms calculated for the oceanic (OCE; bottom) and island arc (ISL; middle) structural models are compared with the data (top). Here the number beneath the identification (station, or model for synthetics) shows the peak-to-peak amplitude (cm).

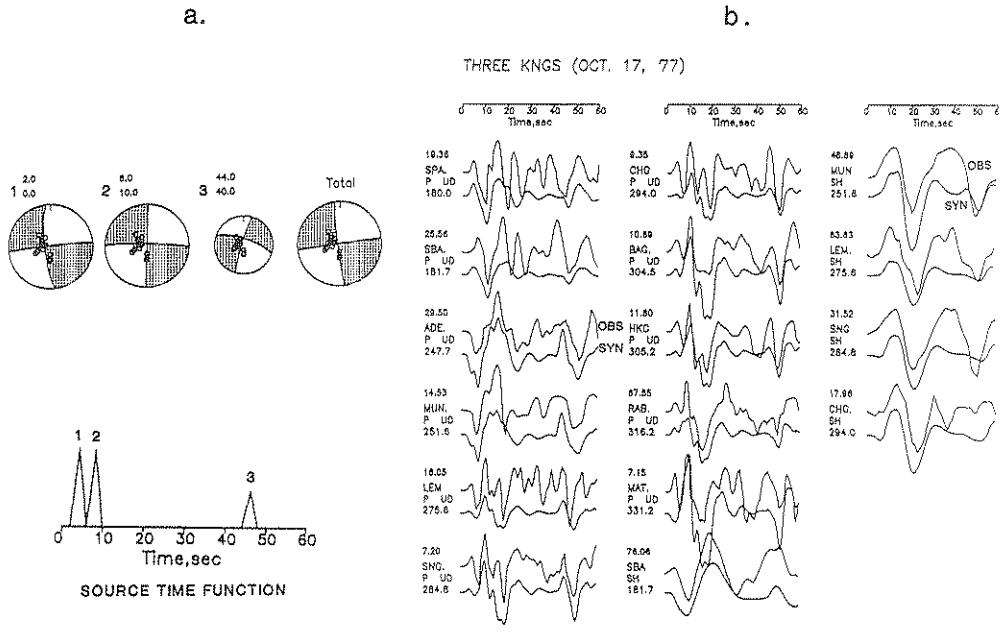


Fig. 8. Inversion results with an island arc crustal velocity model. (a) Source-time function and subevent mechanisms. (b) Comparison between the data (top traces) and synthetics using the rupture model determined by the inversion (bottom traces).

slip ($\phi = 262°$, $\delta = 89°$, $\lambda = 4°$). The total moment release is $2.2 \times 10^{26}$ dyn cm.

Some of the onset amplitudes are small at stations near the nodal planes and the later arriving waveforms, which are probably water phases in the P wavetrains, are not modeled well. Otherwise the synthetic waveforms fit the data reasonably well (see Fig. 8(b)). As the dip angles of these subevents are steeper than 55°, inversion was performed again for the grids with a dip angle of 87° and a strike of 263°. The mechanism parameters and the total moment release have

Table 1
Comparison between the present solution and CMT solution

| Source of solution | Present study | CMT |
|---|---|---|
| Data | WWSSN long-period P and SH waveforms | Long-period ($t_0 > 45$ s) body and mantle waves |
| Subevents | *Grid 1: $\phi = 258°$, $\delta = 55°$*<br>1: $\phi = 263°$, $\delta = 87°$, $\lambda = 11°$; 17 km<br>2: $\phi = 272°$, $\delta = 85°$, $\lambda = 0°$; 17 km<br>3: $\phi = 289°$, $\delta = 72°$, $\lambda = -173°$; 12 km<br>*Grid 2: $\phi = 263°$, $\delta = 87°$*<br>1: $\phi = 262°$, $\delta = 89°$, $\lambda = 9°$; 17 km<br>2: $\phi = 269°$, $\delta = 87°$, $\lambda = -2°$; 17 km<br>3: $\phi = 289°$, $\delta = 71°$, $\lambda = -173°$; 12 km | (NA) |
| Mechanism solution and total moment | $\phi = 262°$, $\delta = 89°$, $\lambda = 4°$ (on Grid 1)<br>$M_0 = 2.2 \times 10^{26}$ dyn cm<br>$\phi = 81°$, $\delta = 89°$, $\lambda = -1°$ (on Grid 2)<br>$M_0 = 2.3 \times 10^{26}$ dyn cm<br>(from the tensorial sum) | $\phi = 258°$, $\delta = 55°$, $\lambda = 0°$; 17.4 km<br>$M_0 = 3.7 \times 10^{26}$ dyn cm |

changed slightly but the locations in the grid and onset times remained unchanged. The mechanisms of the three subevents are: $\phi = 262°$, $\delta = 89°$, $\lambda = 9°$ (Event 1); $\phi = 269°$, $\delta = 87°$, $\lambda = -2°$ (Event 2); $\phi = 289°$, $\delta = 71°$, $\lambda = -173°$ (Event 3). The moments of the individual subevents are found to be $1.3 \times 10^{26}$ dyn cm, $1.4 \times 10^{26}$ dyn cm, and $6.0 \times 10^{25}$ dyn cm, respectively. The mechanism obtained from the tensorial sum of the three subevents is $\phi = 81°$, $\delta = 89°$, $\lambda = -1°$, and the scalar moment is $2.3 \times 10^{26}$ dyn cm. Table 1 summarizes the results of the present study in comparison with the CMT solution.

The rupture velocity estimated from the first two subevents is 2.5 km $s^{-1}$ and that between the second and third subevents is about 1 km $s^{-1}$, which is substantially slower. Here we should note that the design of the body waveform inversion (Kikuchi and Kanamori, 1991) is to model a source process with a series of subevents, whose frequency band is characterized by a given unit source-time function. The duration time of a unit source-time function can vary within the reasonable range of response of the instruments which record data. In the present study, the P waves are complex and characterized by relatively short-period waveforms (less than 10 s), so that we used a triangle unit source-time function defined by $\tau_1 = 2$ s and $\tau_2 = 2$ s. When the unit source-time function is set to have a short duration time, this procedure may not resolve a slow change of mechanism in a single event, even though a series

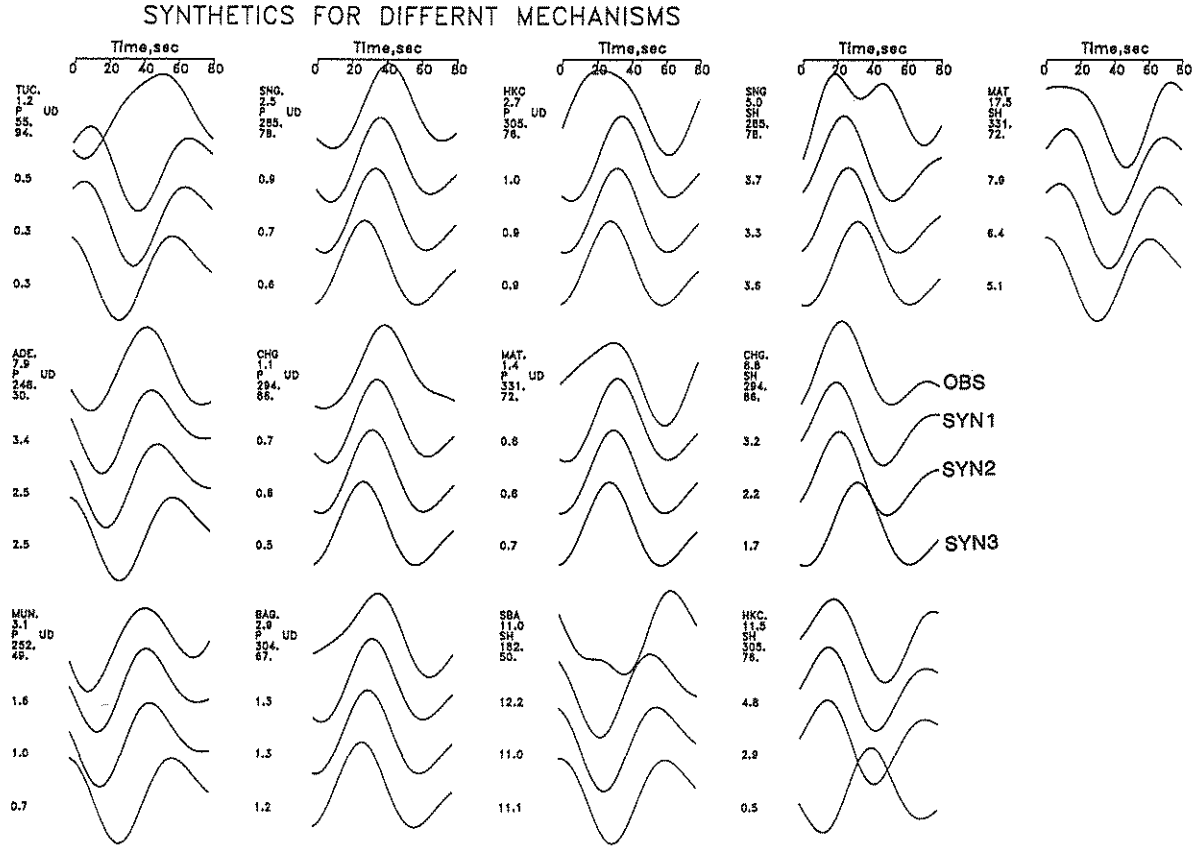


Fig. 9. Synthetic waveforms calculated with three sets of focal parameters are compared with the data (top): (1) the CMT solution (second from top, SYN1); (2) same as (1) but with a steeper dip angle 70° (third from top, SYN2); (3) the solution obtained from the tensorial sum in the present study (bottom, SYN3). The amplitudes of the synthetics are normalized to the corresponding observed waves.

of subevents separated by large intervals may be deconvolved.

### 3.3. Test for low-frequency body waves

Next we tested the low-frequency features by forward modeling the body waveforms using a long-lasting trapezoidal source-time function ($\tau_1$, $\tau_2 = 15$ s, 25 s) for three different sets of mechanisms: (1) the CMT solution; (2) same as (1) but with a steeper dip angle, 70°; (3) using the mechanism parameters from the present study (Fig. 9). Here the scalar moment used is $2.0 \times 10^{26}$ dyn cm. For Mechanisms (1) and (2) the agreement of the P waveform data and synthetics is good at ADE, MUN, SNG, CHG, and BAG, as is the fit of the SH waveforms at CHG, HKC, and MAT. For Mechanism (3) the waveform fit deteriorates as compared with those for Mechanisms (1) and (2). The poor agreement of the P waveforms at TUC and of the SH waveforms at HKC indicates their locations near the nodal planes. The overall amplitudes of the data are two to three times as large as the synthetics except at SBA. This implies that the total moment release estimated in the low-frequency range can be similar to the estimate by the CMT solution.

In summary, the detailed modeling of the teleseismic body waves requires a crustal thickness of about 18 km, in agreement with recent interpretations of the Three Kings Ridge as a remnant volcanic arc. The change of the mechanism in different frequency bands indicates some sort of evolution of the rupture mechanism with time. The source depth of 17 km determined using this crustal structure can be interpreted in the framework of the thermal evolution of the lithosphere. The complex pattern of magnetic anomalies in the vicinity of the northern end of the Three Kings Ridge has been unraveled by Malahoff et al. (1982), who dated the nearby Fiji Basin to Chron 7 or 8 (25–27 Ma). Rheological models of the strength of the lithosphere suggest that brittle rupture could take place at those ages down to approximately 23 km (Wiens and Stein, 1983, 1985). In this respect, the focal depth of the Three Kings event would not be anomalous, even if it were to have occurred in standard oceanic lithosphere.

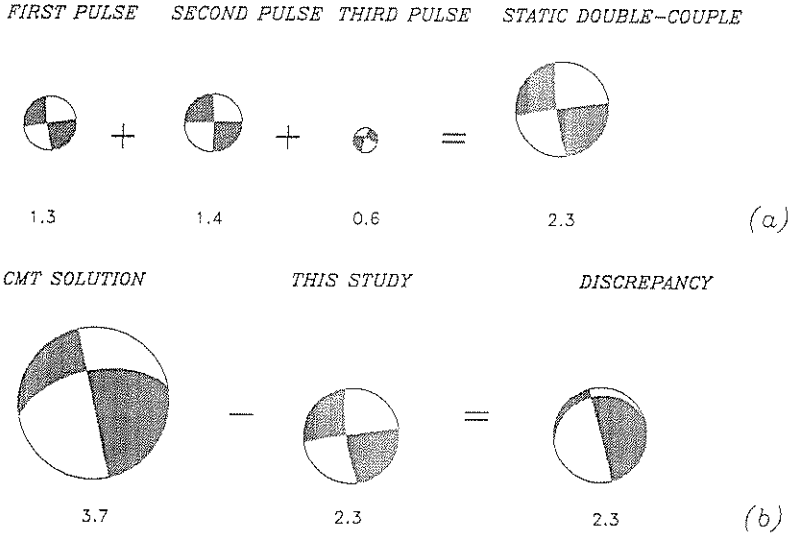


Fig. 10. (a) Focal mechanisms of the three subevents determined in our body-wave inversion and the best-double-couple solution obtained from the tensorial sum of the three subevents' moments. (b) The best-double-couple source for the discrepancy moment tensor between the CMT solution and the solution of our body-wave analysis. Here the radius of each focal sphere is proportional to the moment.

## 4. Low-frequency aspect of the source

### 4.1. CMT solution

Fig. 10 offers a simplified sketch of the relationship between the various sources involved. In the top part (a), we show beachballs for the three subevents, their radius scaled by the scalar value of the moment. The right-hand-side symbol is the major double-couple component of the tensor resulting from the tensorial sum of the moments of the three subevents. We are justified in sketching it as a beachball by the negligible amplitude of its minor double-couple (less than 1%). This mechanism, expressing the static or very-long-period character of the source, is a near perfect strike-slip of moment $2.3 \times 10^{26}$ dyn cm.

It is then interesting to compare this static solution with the Harvard CMT moment tensor (Fig. 10(b)). As the latter has a negligible minor double-couple (less than 1%), we consider only the major double-couple, represented by the large beachball at the left of Fig. 10(b). The difference between that solution and our static moment is shown at right. We call it the 'discrepancy tensor'. Here again, the minor double-couple is negligible (about 4%) and the tensor can be modeled as a double-couple with parameters $\phi = 345°$, $\delta = 89°$, $\lambda = 251°$, and a moment of $2.3 \times 10^{26}$ dyn cm. As shown in Fig. 10(b), this solution approaches a perfect dip-slip on a vertical fault. In other words, the discrepancy between the published CMT solution and the present one is dominated by moment tensor components $M_{r\theta}$ and $M_{r\phi}$: in the

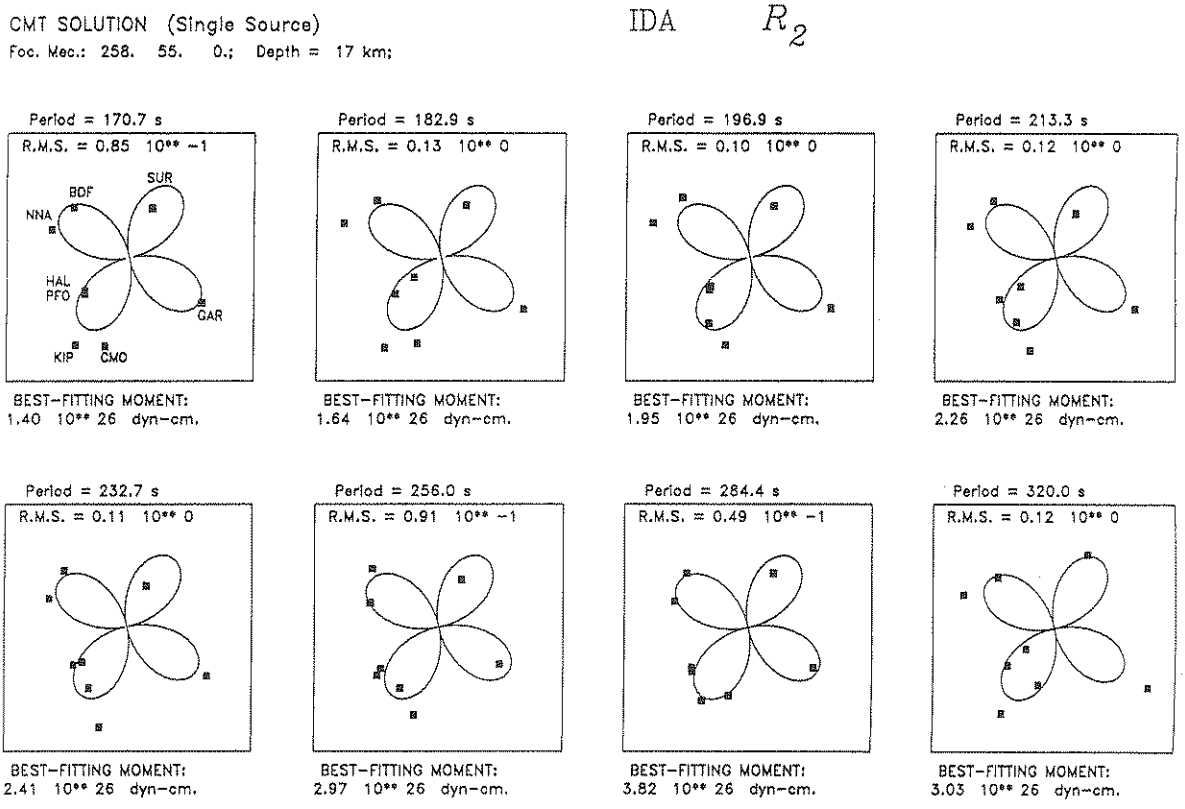


Fig. 11. Equalized spectral amplitude of Rayleigh waves from the 1977 Three Kings earthquakes, as recorded on IDA instruments. In each diagram, the square symbols represent the amplitudes of the spectral amplitudes of the phase $R_2$, plotted at as a function of take-off azimuth, and compared with the theoretical radiation pattern computed either for (a) the CMT solution or (b) our solution. The values of the corresponding best-fitting moments are shown, together with the quality of the fit, as defined by the r.m.s. given by (1).

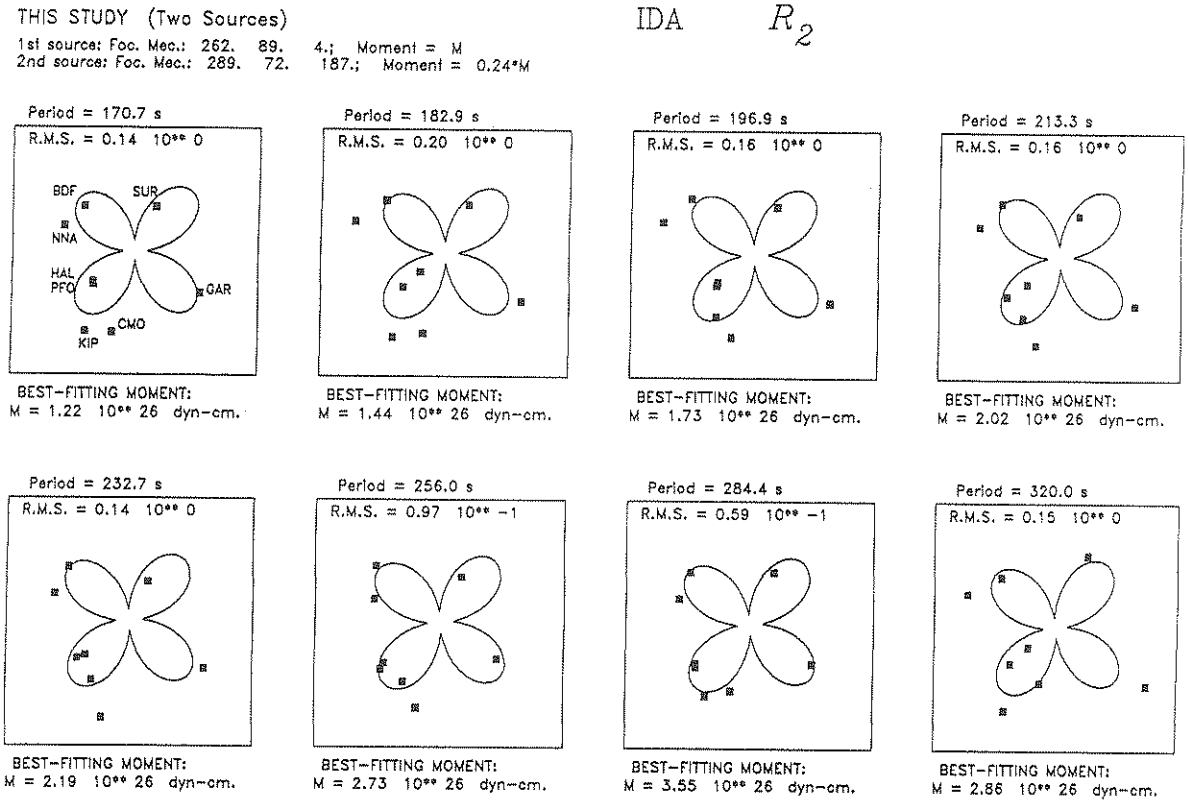


Fig. 11 (continued).

case of a shallow source, these components are notoriously unresolvable because of their vanishing excitation of long-period surface waves (Kanamori and Given, 1981), leading to singularity of the inversion kernels (see also Scott and Kanamori (1985)). In this respect, it is interesting to note that the CMT solution for the Three Kings event was derived from a dataset comprised of 18 45-s body-wave components at seven stations and 32 135-s surface-wave trains at 17 stations (Dziewonski et al., 1987); thus, the inversion was carried out primarily at low frequencies, where the geometry of the discrepancy tensor makes it unresolvable.

### 4.2. IDA data

The Three Kings earthquake was recorded by eight IDA stations. To examine further the uncertainty of the solution, we investigated the amplitude spectra of IDA records of this event. Figs. 11(a) and 11(b) show azimuthal plots of the equalized spectral amplitudes of the phase $R_2$. It was not possible to use $R_1$, owing to non-linear effects at many stations. Furthermore, in 1977, the sampling rate of the IDA stations was 20 s, which in practice limits our frequency coverage to $T \geqslant 160$ s. For each of the Fourier periods between 170 s and 320 s, spectral amplitudes $X(\omega)$ were equalized to a distance of 270°, and compared with their theoretical values, as predicted from the CMT solution (Fig. 11(a)) or from our model inverted from body waves (Fig. 11(b)). In Fig. 11(a), the best-fitting moment $M_0$ is simply obtained by taking the geometrical average of the ratios $X_i^{\text{observed}}(\omega)/X_i^{\text{synthetic}}(\omega)$ at each station $i$. Also given is the (minimized) root-mean-square residual:

$$\sigma = \left\{ \frac{1}{8} \sum_{i=1}^{8} \left[ \log_{10} \frac{X_i^{\text{observed}}(\omega)}{M_0 X_i^{\text{synthetic}}(\omega)} \right]^2 \right\}^{1/2} \qquad (1)$$

This number gives an estimate of the scatter (in magnitude units) in the estimates of the earthquake's size which would be obtained at various stations. In Fig. 11(b), the synthetics have been computed for a combination of sources having the spatial, time and size relationships derived from our body-wave deconvolution experiment. Because of their short spatial and lateral separation, the first two pulses are combined into a unique pulse. The best-fitting moment, $M$ listed for each period is that of the combined first two pulses; the third pulse is given a moment 0.24 $M$.

In general, the fit between the observed and synthetic seismograms is fair, but there is no perceptible improvement between Figs. 11(a) and 11(b). This confirms that the discrepancy between our model and the CMT solution may not be resolved precisely at such low frequencies although our detailed seismological investigations indicate that the Three Kings earthquake consisted of a complex series of shocks with primarily strike-slip focal mechanisms.

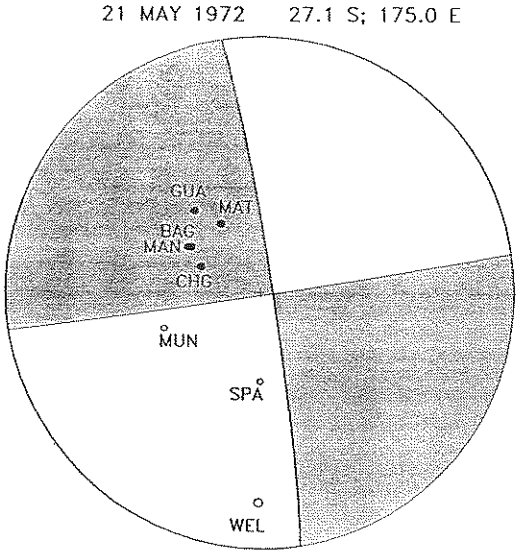


Fig. 12. P-Wave first motions for the nearby 21 May 1972 earthquake. The mechanism plotted shares its east–west-striking fault plane with the static moment of the 1977 event, with the slip angle slightly adjusted (to $-4°$), to reflect the emergent dilatation at SPA.

## 5. Other significant events

Before discussing the tectonic implications associated with the Three Kings earthquake, we briefly describe other significant events in the region. Four other CMT solutions are available in the intraplate area as shown in Fig. 1(b). One earthquake, on 20 May 1982, took place only 91 km WNW of the Three Kings event along the Cook Fracture Zone; its mechanism is generally similar to our solution for the Three Kings event, but its moment remains much smaller ($6 \times 10^{24}$ dyn cm). The other three events, also characterized by strike-slip motion, are located on the Norfolk Rise (17 December 1988) and on the western flank of that structure (26 July 1987 and its next-day aftershock).

Among the WWSSN-era events (1963–1976), only one earthquake was large enough to allow a first-motion focal mechanism study: the 21 May 1972 event ($m_b = 5.6$) located 220 km NE of the Three Kings epicenters. Fig. 12 shows that the mechanism cannot be totally constrained, but a strike-slip solution grossly similar to the Three Kings mechanism would satisfy the available dataset.

Regarding historical earthquakes, we note that three events in 1956, 1957 and 1960 were given Pasadena magnitudes of $6\frac{1}{8}$, 6 and $6\frac{5}{8}$, respectively, the last comparable with the Three Kings event's reported magnitudes. Adams (1972) proposed a magnitude of 'at least 6 to $6\frac{1}{2}$' for the 1960 earthquake, based on the number of reporting stations. These events are shown as inverted triangles in Fig. 1(b). Together with three aftershocks of the 1960 earthquake, they are the only pre-WWSSN earthquakes reliably located in the South Fiji Basin (Valenzuela and Wysession, 1993). However, a direct comparison of these shocks, as recorded on the same instrument (the Benioff 1-90 vertical instrument at Pasadena) suggests that the earthquakes in 1957 and 1960 are significantly smaller than the 1977 event (Fig. 13; only minor traces could be observed for the 1956 earthquake).

In the absence of focal mechanism information, we quantified the 1957 and 1960 events using the formalism of the mantle magnitude $M_m$ (Okal and Talandier, 1989). We obtained $M_m = 6.70$ for the 1977 earthquake, and after correction for focal mechanism and depth, $M_c = 6.38$, suggesting $M_0 = 2.4 \times 10^{26}$ dyn cm, in excellent agreement with the result of body waveform analysis. $M_c$ is a corrected value of the mantle magnitude $M_m$ under the assumption of a particular focal mechanism and a source depth, and it is expected to represent $\log_{10} M_0 - 20$. For the 1960 event on the Norfolk Rise, and given the long-period noise present that day, we restricted our period coverage to $T \leq 130$ s, and obtained $M_m = 6.58$ at 85 s. Assuming a mechanism similar to the nearby 1988 CMT solution, this would result in $M_c = 6.23$, equivalent to a moment of $1.7 \times 10^{26}$ dyn cm. The recording of four aftershocks in the immediate vicinity of the 1960 epicenter confirms the size of this earthquake. Finally, for the 1957 earthquake northwest of the Three Kings epicenter, we found $M_m = 6.23$. Assuming a strike-slip mechanism similar to the 1977 mechanism (also in agreement with the 1982 CMT solution), this translates into $M_c = 5.92$ or a moment of $8 \times 10^{25}$ dyn cm.

## 6. Discussion and conclusions

The above observations suggest that the deformation of the South Fiji Basin concentrates on or along the Norfolk Rise and the Cook Fracture Zone. Along the Cook Fracture Zone, most of the focal mechanisms are strike-slip, and the fault ruptures appear to be en échelon. Pelletier and Louat (1989a,b) have discussed the difference in the opening rate of the South Fiji basin between its northern and southern segments, as separated by the Louisville Ridge intersection with the Tonga–Kermadec Trench, around 26°S, 175°W. They proposed that the Lau Basin to the north opens at 8 cm year$^{-1}$ (full rate), whereas the Havre Basin to the south opens only at 2 cm year$^{-1}$. In their model, they used a rigid Australian plate, and made up for this difference in opening rates by requiring vastly different rates of subduction along the Tonga and Kermadec segments of the trench. Recent measurements of

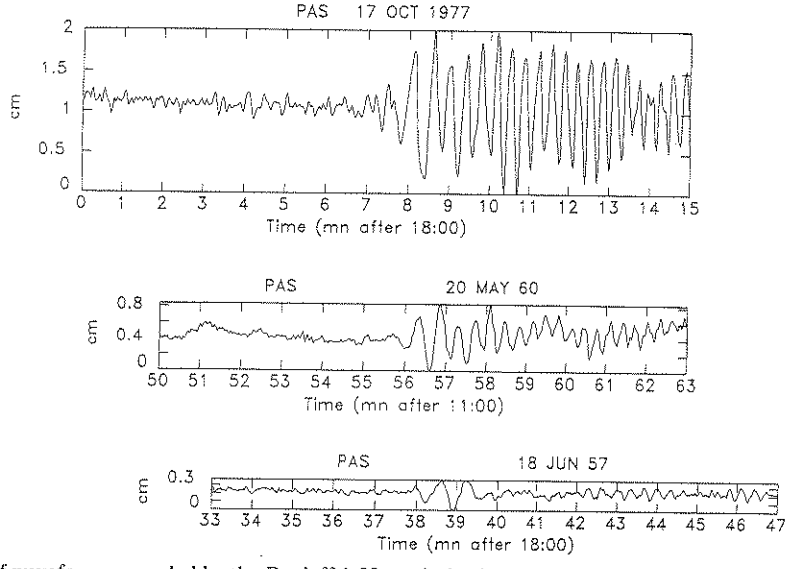


Fig. 13. Comparison of waveforms recorded by the Benioff 1-90 vertical seismometer at Pasadena for the 1977 Three Kings, the 20 May 1960, and the 18 June 1957 earthquakes. The time scales have been lagged to align the group times corresponding to the Airy phase of the Rayleigh wave. The vertical scales are common to all three seismograms.

crustal motion along the Tonga Trench using the global positioning system (GPS) in 1988, 1990, and 1992 show even a larger back-arc spreading rate of about 16 cm year$^{-1}$ in the Lau Basin (Bevis et al., 1993).

Previous studies of magnetic anomalies suggest a distinction between the southern section and the northern half of the South Fiji Basin (Malahoff et al., 1982). The bathymetric features also indicate a different tectonic history of this basin between the two sections, which appear to be separated by an eastward extension of the Cook Fracture Zone. The Three Kings earthquake and the neighboring seismicity take place along the westwards extension of the Louisville Ridge intersection, and of the change of subducting and spreading regime. The level of moment release documented along the Cook Fracture Zone system is relatively minor (at most $(3–4) \times 10^{26}$ dyn cm over 35 years), and may not be large enough to argue against Pelletier and Louat's (1989b) model, which assumed the entire region as a rigid portion of the Australian plate. Nevertheless, we think that the Three Kings earthquake can be interpreted as evidence of a minor level of internal deformation of the plate, consistent with the different rates of spreading in the Lau and Havre Basins.

Tectonic models published for this region are somewhat speculative, owing to the very complex plate tectonics history of the area (Yang and Kroenke, 1993), and to some extent to the limitation of the local seismographic coverage. The various models proposed to explain the origin of structures such as the Three Kings Ridge were obtained on the basis of seismic reflection profiles (e.g. Kroenke and Dupont, 1982). The establishment of broad-band seismic stations, on either a permanent or a temporary basis, would allow the systematic waveform modeling of small events, and a number of tomographic studies in the area, which should shed additional light on the structure of the crust and upper mantle in the area. At present, one only broadband station (Nouméa) is within 1000 km of the 1977 epicenter.

In conclusion, body waveforms from the Three Kings Ridge 1977 earthquake indicate that the source is composed of three subevents, and that both the geometry and the total moment release were significantly different from those given by the CMT inversion. Although we understand the origin of the discrepancy, our study illustrates some level of evolution of the mechanism with time and also a possible systematic bias in the CMT solutions. The moment release of this event is clearly above the level of the background seismicity in this oceanic basin, which indicates a substantial amount of deformation of that portion of the Australian plate. Finally, our body-wave modeling at frequencies significantly higher than those used in the CMT solution requires a crustal source, which in turn indicates that crust in the source region is thicker than an ordinary oceanic crust, in agreement with the suggestion, obtained in previous studies using different approaches, that the Three Kings Ridge is a fossil volcanic arc.

## Acknowledgments

F. Taylor and P. Mann provided us with useful information on the tectonics in the South Fiji Basin. R. Louat pointed out the varying plate convergence rate in the South Fiji basin. D. Schaff worked out the focal mechanism of the 1972 event; we thank M. Wysession for sending us a complete file of relocated epicenters, prior to publication, and L. Kroenke for a private Honolulu preview of his animated reconstruction. The comments by the anonymous reviewers helped improve the clarity of the manuscript. This study was partially supported by NSF Grants EAR-8916458 and EAR-9304652.

## References

Adams, R.D., 1972. An earthquake to the northwest of New Zealand. N.Z.J. Geol. Geophys., 15: 674–677.

Bergman, E.A. and Solomon, S.C., 1980. Oceanic intraplate earthquakes: implication for local and regional intraplate stress. J. Geophys. Res., 85: 5389–5410.

Bevis, M., Taylor, F.W., Schultz, B.E. and Calmant, S., 1993. Geodetic observation of convergence and back arc spreading in the S.W. Pacific (1988–1992). EOS Trans. Am. Geophys. Union, 74: 60.

Coleman, P.J. and Packham, G.H., 1976. The Melanesian borderlands and India–Pacific plates boundary. Earth-Sci. Rev., 12: 197–233.

Dziewonski, A.M., Ekström, G., Franzen, J.E. and Woodhouse, J.H., 1987. Global seismicity of 1977; centroid moment tensor solutions for 471 earthquakes. Phys. Earth Planet. Inter., 45: 11–36.

Kanamori, H. and Given, J.W., 1981. Use of long-period surface waves for rapid determination of earthquake-source parameters. Phys. Earth Planet. Inter., 27: 8–31.

Karig, D.E., 1972. Remnant arcs. Geol. Soc. Am. Bull., 83: 1057–1068.

Kennett, B.L.N. and Engdahl, E.R., 1991. Travel times for global earthquake location and phase identification. Geophys. J. Int., 105: 429–465.

Kikuchi, M. and Kanamori, H., 1991. Inversion of complex body waves—III. Bull. Seismol. Soc. Am., 81: 2335–2350.

Kroenke, L.W. and Dupont, J., 1982. Subduction–obduction: a possible north–south transition along the west flank of the Three Kings Ridge. Geo-Mar. Lett., 2: 11–16.

Kroenke, L.W. and Eade, J.V., 1982. Three Kings Ridge: a west-facing arc. Geo-Mar. Lett., 2: 5–10.

Launay, J., Dupont, J. and Lapouille, A., 1982. The Three Kings Ridge and the Norfolk Basin (Southwest Pacific): an attempt at structural interpretation. South Pac. Mar. Geol. Notes, 2: 121–130.

Malahoff, A., Feden, R.H. and Fleming, H.S., 1982. Magnetic anomalies and tectonic fabric of marginal basins north of New Zealand. J. Geophys. Res., 87: 4109–4125.

Mammerickx, J., Smith, S.M., Taylor, T.L. and Chase, T.E., 1974. Bathymetry of the South Pacific, map. Scripps Institution of Oceanography, University of California, La Jolla.

Okal, E.A. and Talandier, J., 1989. $M_m$: a variable period mantle magnitude. J. Geophys. Res., 94: 4169–4193.

Packham, G.H. and Terrill, A., 1975. Submarine geology of the South Fiji Basin. Initial Reports of the Deep Sea Drilling Project, 30. US Government Printing Office, Washington, DC, pp. 617–645.

Pelletier, B. and Louat, R., 1989a. Mouvements relatifs des plaques dans le Sud-Ouest Pacifique, C.R. Acad. Sci. Paris. Sér. II, 308: 123–130.

Pelletier, B. and Louat, R., 1989b. Seismotectonic and present-day relative plate motions in the Tonga–Lau and Kermadec–Havre region. Tectonophysics, 165: 237–250.

Scott, D.R. and Kanamori, H., 1985. On the consistency of moment tensor source mechanisms with first-motion data. Phys. Earth Planet. Inter., 37: 97–107.

Valenzuela, R.W. and Wysession, M.E., 1993. Intraplate earthquakes in the Southwest Pacific Ocean Basin and the seismotectonics of the Southwest Tasman Sea. Geophys. Res. Lett., 20: 2467–2470.

Van der Linden, W., 1969. Extinct mid-ocean ridges in the Tasman Sea and in the Western Pacific. Earth Planet. Sci. Lett., 6: 483–490.

Wiens, D.A. and Stein, S., 1983. Age dependence of oceanic intraplate seismicity and implications for lithospheric evolution. J. Geophys. Res., 88: 6455–6468.

Wiens, D.A. and Stein, S., 1985. Implications of oceanic intraplate seismicity for plate stresses, driving forces and rheology. Tectonophysics, 116: 143–162.

Yang, C.-Y. and Kroenke, L.W. 1993. A plate reconstruction of the Southwest Pacific, 0–100 Ma. Proc. Ocean Drilling Program, Scientific Results, 130. Ocean Drilling Program, College Station, TX, pp. 697–709.